Int J Fract (2016) 197:63–79
DOI 10.1007/s10704-015-0061-y

ORIGINAL PAPER

Mixed-mode fracture of layered plates subjected to in-plane bending

Servesh Kumar Agnihotri · Venkitanarayanan Parameswaran

Received: 8 August 2015 / Accepted: 7 December 2015 / Published online: 15 December 2015

Abstract Layered architecture is being widely used in applications such as thermal protection systems, windshields, body and vehicle armor etc. In layered materials, properties vary in a discrete manner from layer to layer, leading to property jumps across the interfaces. The focus of this study is to understand the mixed mode fracture behavior of cracked layered plates in which elastic and fracture properties vary along the crack front. Layered plates were prepared by joining polymethylmethacrylate (PMMA) and Epoxy sheets using an Epoxy based adhesive (Araldite). Between the two materials, Epoxy has higher elastic modulus and lower fracture toughness. Single edge notched specimens were subjected to asymmetric four point bending. The failure was observed to be progressive in nature with the crack in Epoxy layer extending first followed by crack growth in PMMA layer. Inspection of fractured surfaces indicated twisting of crack during crack extension. Results of three-dimensional finite element analysis (FEA) indicated variation of SIF and mode mixity along the crack front and also presence of mode-III SIF. The load corresponding to extension of crack and angle of crack propagation in the Epoxy layer was reasonably predicted by the maximum tensile stress criteria. The interaction between the two layers once the crack in the Epoxy layer starts growing is explained using results of FEA.

S. K. Agnihotri (✉) · V. Parameswaran
Department of Mechanical Engineering, Indian Institute of Technology Kanpur, Kanpur 208016, India
e-mail: servesh@iitk.ac.in

Keywords Layered plates · Stress intensity factors · Photoelasticity · Fracture · Crack twisting · Mixed-mode

1 Introduction

In recent years, layered structures have received considerable attention due to their potential use in applications such as windshields, heavy armor, thermal protection systems etc. Layered materials offer the designer the flexibility to fully integrate individual layer properties and impart the required overall properties in the layered structure. However, the presence of property jumps at layer interfaces brings additional complexities in their failure behavior. In general, fracture behavior of a layered structure can be influenced by the change of elastic and fracture properties from layer to layer, type of loading experienced and orientation of the crack.

Fracture behavior of layered materials has been addressed by many researchers. There exists extensive literature addressing the fracture behavior of bi-material systems consisting of two dissimilar materials. These studies investigated the behavior of (i) stationary crack oriented along the interface (Rice and Sih 1965; Hutchinson and Suo 1992; Xu and Tippur 1995) (ii) cracks propagating along the interface (Tippur and Rosakis 1991; Yang et al. 1991; Liu et al. 1993; Singh and Shukla 1996; Singh et al. 1997; Shukla and Kavaturu 1998; Shukla 2001) and (iii) crack propagation across the interface (Erdogan and Biricikoglu

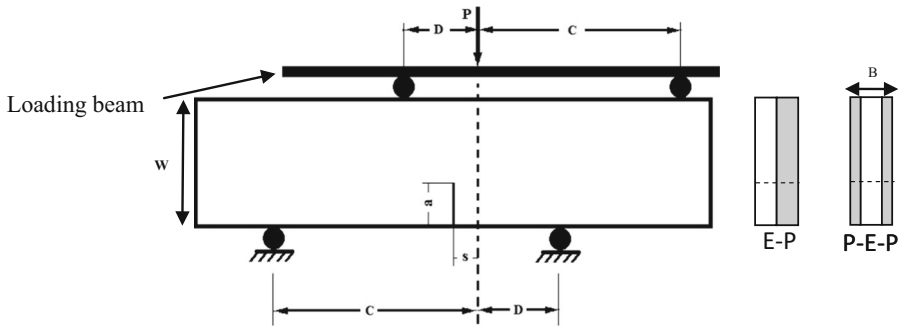

Fig. 1 Asymmetric four point bending configuration

1973; Singh and Parameswaran 2003); Parameswaran and Shukla 1998). Relatively, the behavior of a through thickness edge crack in a layered plate having jumps in both elastic and fracture properties along the crack front has received very less attention. An approximate three dimensional theory for layered plates having a through thickness crack, developed by Badaliance and Sih, indicated that the near tip fields in each layer are identical to that in a homogeneous plate (Badaliance and Sih 1975). Recently Kidane and Shukla (2010) have reported fracture initiation toughness of Ti/TiB layered graded material as a function of temperature under quasi-static and dynamic loading. They performed two types of fracture tests, one in which the property variation is along the length of the crack and the other in which the crack front cuts through the layers leading to property jumps along the crack front. Very recently, Bankar and Parameswaran (2013) investigated the opening mode fracture of edge cracked layered plates subjected to in plane bending. They observed that the stress intensity factor (SIF) was higher in the relatively stiffer layer because of which crack initiated first in this layer. Interestingly, due the layered configuration, the crack in the stiffer layer extended stably to some distance before final failure of the plate.

In this study, the behavior of an edge crack in a layered plate subjected to mixed mode loading is investigated. The same layered system consisting of two different polymers, Epoxy (LY556) and polymethylmethacrylate (PMMA) reported in Bankar and Parameswaran (2013) is used. The asymmetric four point bending (AFPB) configuration is used to generate different levels of mode mixity in the specimen. Thickness averaged SIF is measured using photoelasticity. The fracture surfaces of the tested specimen are mapped to understand the path followed by the crack in different layers. Further, detailed three-dimensional finite element (FE) analysis is also performed to understand the mechanics involved and to explain the experimental observations.

2 Experimental details

2.1 Specimen preparation and characterization

A layered plate comprising of two material systems, Epoxy and PMMA, is considered in this study. The specimens were fabricated by bonding Epoxy and PMMA sheets using an Epoxy based adhesive (Araldite). The motivation for choosing Epoxy and PMMA is that both materials are transparent and birefringent. Transparencies of these materials allow one to clearly observe the fracture path. Further, birefringent nature of these materials facilitates the use of photoelasticity to visualize the stress field and to measure the through thickness average of the SIF. PMMA sheets of nominal thickness 5.5 and 2.7 mm were commercially procured. Epoxy sheets of nominal thickness 5.8 mm were cast in-house. The details of the casting procedure and bonding of Epoxy and PMMA sheets were reported in Bankar and Parameswaran (2013). Plates having two different configurations as shown in Fig. 1 were prepared. In the first configuration, referred to as E–P plate, a single layer of Epoxy was bonded to a single layer of PMMA. In the second configuration, referred to as P–E–P plate, a single layer of Epoxy was sandwiched between two layers of PMMA of nominal thickness 2.7 mm. Both configurations therefore had the same final thickness. Single edge notched (SEN) specimens of size 225 × 50 mm were machined out of the plates. A notch of required length was introduced using a saw and a natural crack was extended by forcing a sharp razor blade into the root of the notch. The measured elastic, fracture and optical properties of Epoxy and PMMA, are given in Table 1.

Table 1 Properties of materials used

Material	Elastic modulus (GPa)	Poisson's ratio	Fringe constant (MPa-m/fringe)	Fracture toughness (MPa-$\sqrt{}$m)
PMMA	2.67	0.344	0.240	0.95 ± 0.11
Epoxy	4.16	0.350	0.018	0.67 ± 0.09

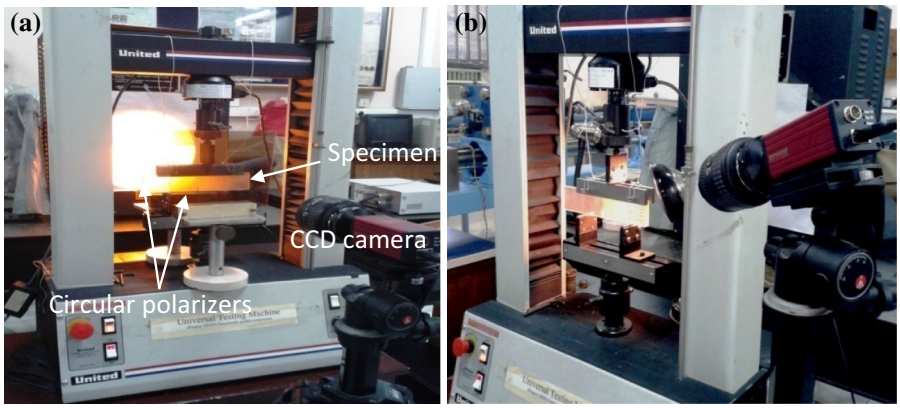

Fig. 2 Photographs of experimental setup for **a** photoelastic experiments, **b** observing crack growth

SEN specimens were subjected to asymmetric four-point bending (AFPB) as shown in Fig. 1 using a universal testing machine having a 25 kN dual bridge load cell. Different levels of mode mixity in loading were obtained by varying the eccentricity (s) between loading axis and crack plane. For the AFPB configuration used, we have chosen the parameters $\frac{C}{W}$ and $\frac{D}{W}$, as 1.6 and 0.8, respectively, where C and D are indicated in Fig. 1. For a single layer plate having a straight edge crack, the mode-I and mode-II SIFs for AFPB can be obtained using the following expressions (Maccagno and Knott 1989).

$$K_I = \frac{M}{BW^{3/2}} Y_I, \quad K_{II} = \frac{Q}{BW^{1/2}} Y_{II}, \tag{1}$$

where W is the width of the plate, B is the thickness of the plate, and Y_I and Y_{II} are respectively the mode I and mode II calibration functions (Maccagno and Knott 1989). M and Q are respectively the bending moment and shear force in the crack plane. In all experiments, an a/W ratio of 0.3 was used. Two sets of experiments were performed. In the first set of experiments, the specimen illuminated by a monochromatic light source was viewed through a circular polariscope during loading as shown in Fig. 2a. The isochromatic fringes were recorded using a two megapixel monochrome CCD camera. In the second set of experiments, the specimen was viewed at an angle, in order to track the growth of the crack front in each layer as shown in Fig. 2b. A square grid consisting of 5 mm squares was imprinted on the front surface of the specimen to facilitate the measurement of the crack length in the second set of experiments. In all the experiments, the images were captured at a time interval of 200 ms. All experiments were carried out at a loading rate of 0.5 mm/min. The image grabbing software records the analogue output from the load cell simultaneously with each image allowing time synchronization between load, load point displacement and the images.

2.2 Analysis of isochromatics

The procedure of extracting the SIF from the isochromatics involves fitting the asymptotic crack tip stress fields to the fringe data using a non-linear least square algorithm (Dally and Riley 1978). Assuming the strains to be invariant through the thickness of an edge cracked layered plate subjected to in plane bending, an equivalent plate approach for analyzing the fringes was presented in Bankar and Parameswaran (2013). For analyzing the fringes under mixed mode loading also we follow the equivalent plate approach in which the layered plate is considered as a homogenous plate of equivalent elastic modulus E_{eq} and equivalent fringe constant $f_{\sigma eq}$. The isochromatics are then analyzed using

the equivalent fringe constant ($f_{\sigma eq}$) calculated using the following equation.

$$\frac{1}{f_{\sigma eq}} = \frac{1}{E_{eq} h_t}\left(\frac{E_p h_p}{f_{\sigma p}} + \frac{E_e h_e}{f_{\sigma e}}\right), \tag{2}$$

where, $f_{\sigma p}$ and $f_{\sigma e}$ denote the optical fringe constant for PMMA and Epoxy respectively, E_p and E_e are respective elastic moduli, h_p and h_e the respective thicknesses and h_t is the total thickness of the plate. The equivalent elastic modulus E_{eq}, is given by

$$E_{eq} = \frac{1}{h_t}\int_0^{h_t} E(z)dz = \frac{1}{h_t}\sum_{i=1}^{n} E_i h_i \tag{3}$$

The near tip stress field in the equivalent plate is assumed to have the structure given by Eq. 4 (Dally and Riley 1978).

$$\sigma_{ij} = \sum_{n=0}^{N} A_n r^{(n-1/2)} f_n(\theta) + \sum_{m=0}^{M} B_m r^m g_m(\theta) - \sum_{n=0}^{N} C_n r^{(n-1/2)} h_n(\theta) - \sum_{m=0}^{M} D_m r^m k_m(\theta), \tag{4}$$

where r and θ denote the polar coordinates of a point with respect to the crack tip and $f_n(\theta)$, $g_m(\theta)$, $h_n(\theta)$ and $k_m(\theta)$ are angular functions, explicit form of which are available in Dally and Riley (1978). The constants A_n, B_m, C_n and D_m in Eq. (4) can be evaluated from isochromatic fringe data using the least square over deterministic method described in Dally and Riley (1978). The opening mode SIF, K_I and sliding mode SIF, K_{II} are related to the coefficients, A_0 and C_0 as shown in Eq. 5.

$$K_I = \sqrt{2\pi} A_0, \quad K_{II} = \sqrt{2\pi} C_0 \tag{5}$$

Mode mixity (Θ), which shows the strength of mode-II stress field relative to mode I field, is then calculated as

$$\Theta = \tan^{-1}\left(\frac{K_{II}}{K_I}\right) \tag{6}$$

The SIF thus obtained is the thickness averaged SIF or equivalent SIF (K_{eq}) for the equivalent homogenous plate. The SIF in each individual layer is given by (Kommana and Parameswaran 2009).

$$K_{e(I,II)} = \frac{E_e}{E_{eq}} K_{eq(I,II)}, \quad K_{p(I,II)} = \frac{E_p}{E_{eq}} K_{eq(I,II)} \tag{7}$$

where, subscripts e and p refer to Epoxy and PMMA respectively.

The SIF and other constants (in Eq. 4) were extracted by sampling the fringe order at a select set of points around the crack-tip and fitting Eq. (4) to this data using the stress-optic law. The accuracy of solution was checked by regenerating the fringes using the extracted coefficients and comparing them with the fringes obtained experimentally.

2.3 Crack growth and propagation direction

Crack propagation direction in the layered plate is calculated using the maximum tangential stress (MTS) criterion (Kumar 2009). MTS criterion states that crack extension will occur along the direction for which the tangential stress component at an infinitesimal radial distance from the crack tip is maximum and the extension will take place when the maximum tangential stress reaches a critical value, which is a material dependent parameter. Crack initiation angle can be obtained by solving Eq. (8) (Kumar 2009).

$$K_I \sin\theta_c + K_{II}(3\cos\theta_c - 1) = 0 \tag{8}$$

Where K_I and K_{II} are mode-I SIF and mode-II SIF respectively and θ_c is the crack propagation angle. The equivalent opening mode SIF is given as (Kumar 2009).

$$K_I^e = K_I \cos^3\left(\frac{\theta_c}{2}\right) - \frac{3}{2} K_{II} \cos\left(\frac{\theta_c}{2}\right) \sin\theta_c \tag{9}$$

The critical condition for crack initiation is attained when

$$K_I^e \geq K_{Ic}, \tag{10}$$

where K_{Ic} is the mode-I fracture toughness of the material considered. The experimentally measured crack propagation angle has been compared with that predicted by MTS criteria. The criticality condition for

crack initiation in the Epoxy layer is also calculated using the MTS criteria.

3 Finite element modeling

Two different FE analyses were performed in this study. A three-dimensional FE analysis in which both layers have cracks of the same length is performed to determine the variation of the SIFs through the thickness of the plate for selected values of s. Further, based on the experimental observation, a three-dimensional FE analysis in which the two layers have cracks of different length was also performed. This analysis was performed to understand the interaction between the layers during progressive cracking of the Epoxy layer. The details of the model, boundary conditions and loading scheme used are presented in subsequent sections. All analyses were carried out using commercial FE software ABAQUS v6.13

3.1 FE model for same length cracks in Epoxy and PMMA layers

Epoxy and PMMA layers were modeled individually conforming to the dimension mentioned in Sect. 2.1. The material properties as mentioned in Table 1 were assigned to each layer. Crack was modeled as a seam, which is a set of overlapping nodes free to move apart under the load. The two layers in E–P plate (or three layers in P–E–P) were assembled using a surface based tie constraint, which provides easy mesh transitioning at the interface. The entire model was meshed with 20 node reduced integration brick elements (C3D20R). The three dimensional view and front view of the two-layer model are shown in Fig. 3. A focused radial mesh (Fig. 4) was generated by partitioning the region around the crack tip into two circles and dividing them into equal parts to obtain crack tip elements of size 50 μm. Except near the free surface and interface between the layers, the elements had a size of 1 mm in the thickness direction. Elements near the free surfaces and on either side of the interface had a size of 50 μm in thickness direction (Fig. 5). Collapsed 20 node elements with quarter point nodes were used along the crack front to capture the square root strain singularity. A separate rigid part having dimension same as the loading beam (refer Fig. 1) in the experimental set up was

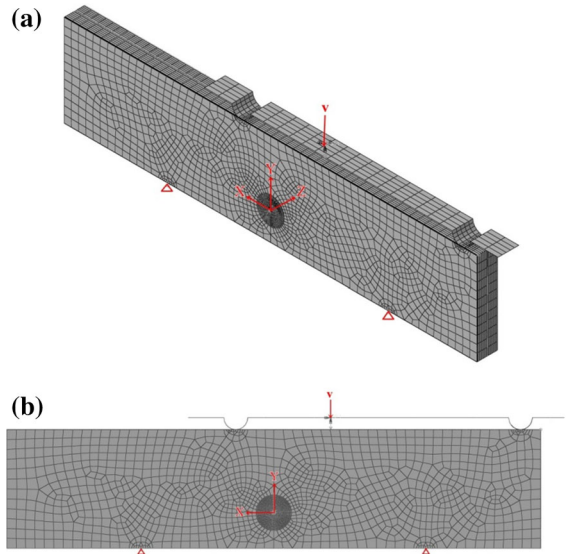

Fig. 3 FE mesh of cracked two layer model **a** three dimensional view, **b** front view

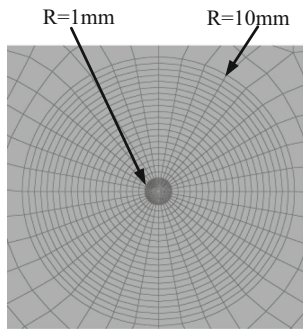

Fig. 4 Radial focused mesh at the crack tip

also modeled to replicate the method of loading used in the experiments. This part was assembled to the specimen using surface based tie constraints. The rotational degrees of freedom of all the nodes lying on the contact line were kept untied. The refined model consisted of 1,37,366 elements and 5,82,284 nodes. A constant downward displacement was applied at the reference point of the loading beam corresponding to the experimental load application point as shown in Fig. 3.

3.2 FE model for different length cracks in Epoxy and PMMA layers

The results from experiments (to be discussed later) indicated that the Epoxy crack propagates some dis-

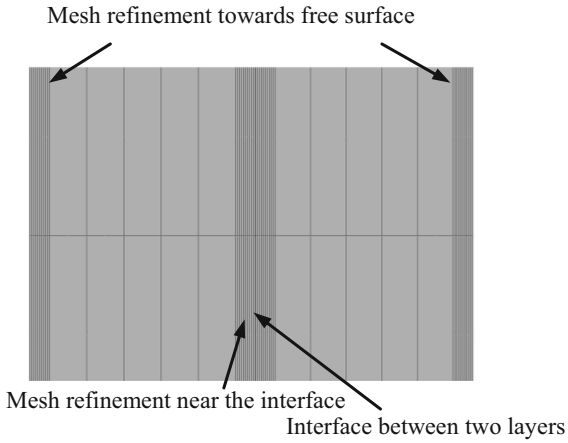

Fig. 5 Mesh refinement along the thickness

tance before PMMA crack initiates. The layered plate has been modeled in this condition (Fig. 6a) where Epoxy and PMMA crack fronts are at different locations. The Epoxy crack kink angle and propagation distance used in the model have been obtained from experiments. For the E–P plate, the length of the Epoxy crack was 18 mm whereas that for the P–E–P plate was 12 mm. Similar meshing scheme as described in Sect. 3.1 was used near the crack tip and at the free surfaces and interfaces. Figure 6b shows the meshing at the two crack tips for the E–P plate. Similarly, the P–E–P plate was also modeled in this condition. This model has been subjected to constant downward displacement corresponding to the load just before the PMMA crack initiation in each case.

3.3 Evaluation of SIF from FE results

Various methods have been proposed to calculate the SIF from finite element results. J-integral and interaction integral are commonly used methods for the calculation of opening mode and mixed mode SIF respectively. Moran and Shih (1987) developed a domain integral method to calculate the J-integral for three dimensional cracks in homogeneous materials. Similar approach was also followed by Walters et al. (2004, 2005) to develop a domain integral for three dimensional cracks in graded materials. They superimposed two different fields i.e. actual (computed) fields and auxiliary fields to evaluate the interaction integral at the crack tip (Walters et al. 2005). Auxiliary fields are chosen as asymptotic fields for pure mode-I, mode-II or mode-III case. J-integral for superimposed states can be written as

$$J^S(s) = J(s) + J^{aux}(s) + I(s) \tag{11}$$

where $J(s)$ and $J^{aux}(s)$ are the domain integral for the actual fields and auxiliary fields respectively and $I(s)$ is the integral interacting with actual and auxiliary terms. The explicit form of the J-integral and interaction integral are given in Walters et al. (2005).

In terms of mixed mode SIFs, the expression for the J-integral for superimposed state can be written as

$$J^S(s) = \frac{1}{E^*}\left[(K_I + K_I^{aux})^2 + (K_{II} + K_{II}^{aux})^2\right] + \frac{1+\nu}{E}(K_{III} + K_{III}^{aux})^2 \tag{12}$$

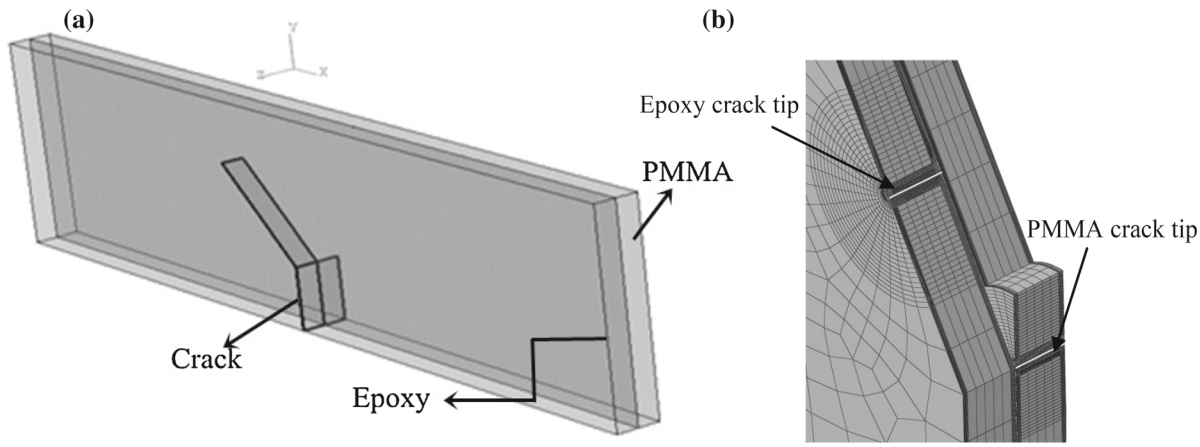

Fig. 6 Crack front in Epoxy and PMMA layer(s) before crack propagation in PMMA layer(s)

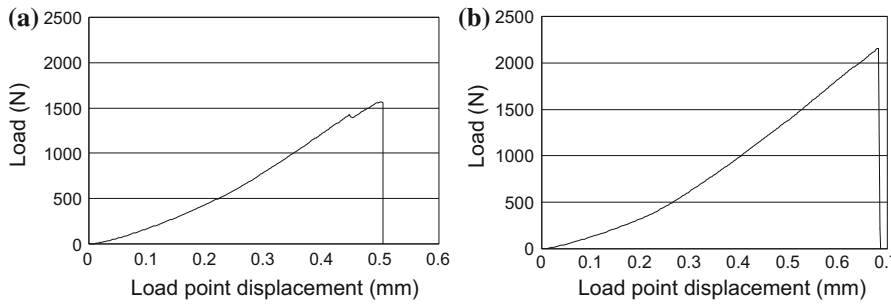

Fig. 7 Load-displacement record for $s = 24$ mm **a** E–P and **b** P–E–P

From Eqs. 11 and 12, the expression for the interaction integral can be deduced as

$$I(s) = \frac{1}{E^*}\left(2K_I K_I^{aux} + 2K_{II}K_{II}^{aux}\right) + \frac{1+\nu}{E}\left(2K_{III}K_{III}^{aux}\right) \tag{13}$$

By making appropriate choices of auxiliary field as pure mode-I asymptotic field with $K_I^{aux} = 1$, $K_{II}^{aux} = 0$, $K_{III}^{aux} = 0$, we can obtain actual mode-I stress intensity factor as

$$K_I = \frac{E^*}{2} I(s) \tag{14}$$

where $E^* = E$ for plane stress and $E^* = \frac{E}{(1-\upsilon^2)}$ for plane strain. Following Nakamura and Parks (1988, 1989), we use $E^* = \frac{E}{(1-\upsilon^2)}$ in Eqs. (13, 14). Similarly mode-II and mode-III SIF can be obtained by choosing the auxiliary fields as pure mode-II and pure mode-III asymptotic field with $K_{II}^{aux} = 1$, $K_I^{aux} = 0$, $K_{III}^{aux} = 0$ and $K_{III}^{aux} = 1$, $K_I^{aux} = 0$, $K_{II}^{aux} = 0$ respectively in Eq. (13) resulting in the following relations.

$$K_{II} = \frac{E^*}{2} I(s), \quad K_{III} = \mu I(s) \tag{15}$$

The standard routine for evaluating interaction integral available in Abaqus was used to obtain the variation of SIFs along the crack front.

4 Experimental results

4.1 Fracture behavior

The experimental results of AFPB test will be discussed in this section. Figure 7 shows typical load-displacement record for $s = 24$ for the E–P and P–E–P plates. The isochromatic fringes corresponding to selected loads for $s = 24$ mm are shown in Fig. 8. As shown in Fig. 7a for E–P plate, the load increases and at a certain point there is a slight drop in the load. The slight drop in the load observed in Fig. 7a is coincident with the first extension of the Epoxy crack. With increase in load, the crack in the Epoxy layer extended through a series of jumps and arrests along the kinked direction to some distance. The isochromatic fringes shown in Fig. 8a indicate that the loading is mixed mode prior to crack extension in the Epoxy layer. However, once the crack in the Epoxy layer extends, the state of stress is predominantly opening mode as indicated by the fringes in Fig. 8b, c. On reaching the maximum load, the crack in the PMMA layer started extending and resulted in sudden failure of the specimen. On the contrary, a drop in load is not observed in Fig. 7b for the P–E–P plate even though the Epoxy layer crack starts extending once the load reaches a certain value. In both cases, on reaching the maximum load, the specimen failed suddenly with cracks in all layers extending unstably. The opening and shear mode SIFs just before Epoxy crack initiation was evaluated by analyzing the isochromatics as explained in Sect. 2.2. The thickness averaged SIFs thus obtained are plotted in Fig. 9 as a function of s along with that obtained using Eq. (1). As expected, mode-I SIF decreases and mode-II SIF increases with decreasing levels of s. The SIF calculated using Eq. (1) is in reasonable agreement with that measured from experiments.

The results of experiments conducted for real-time observation of the crack front progression in the layered plate will be now discussed. Figures 10 and 11 show the photographs of crack front at various stages of loading in E–P and P–E–P plate respectively. There is an initial crack jump in the Epoxy layer followed by crack extension through a sequence of jumps and arrests. The average initial crack jump ($8 \leq s \leq 24$ mm) was 13 ± 3 mm. The total crack advance in the Epoxy layer

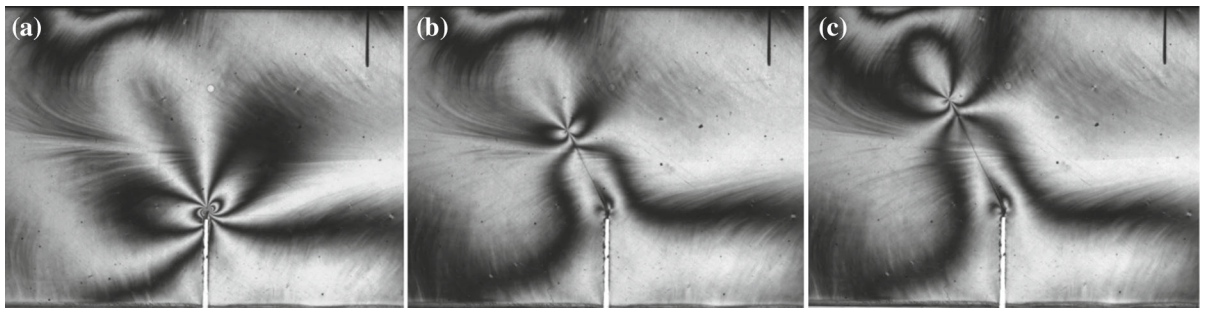

Fig. 8 Isochromatics in E–P plate subjected to asymmetric four-point bending for $s = 24$ mm **a** just before crack jump in Epoxy layer, **b** after crack jump, **c** just before final unstable failure

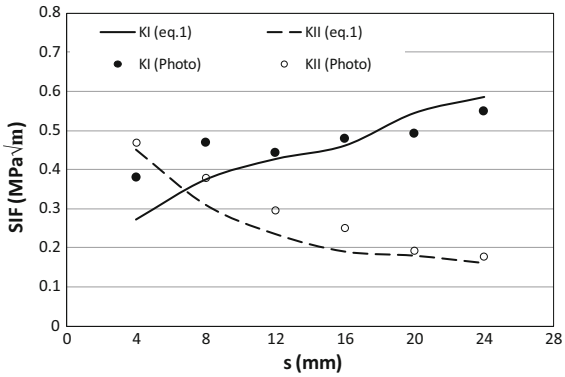

Fig. 9 Comparison of measured SIFs with that obtained from Eq. (1) for different values of s just before extension of Epoxy layer crack

before the PMMA layer crack started advancing varied from 18 mm for lower mode mixity ($s = 24$ mm) to 21 mm for higher mode mixity ($s = 8$ mm). In the case of $s = 4$ mm, the crack growth in both layers occurred simultaneously leading to sudden failure of the specimen. For the E–P plate, it can be observed from Fig. 10 that the crack front in Epoxy layer is not straight. Crack advance in the Epoxy layer is more at locations away from the interface. Crack advances less near the interface due to the closing traction applied by the un-cracked portion of the PMMA plate, resulting in an asymmetric crack front profile.

For the P–E–P plate, the initial crack jump observed was very small and could not be accurately measured with the 5×5 mm^2 grid used. The crack advance in the Epoxy layer before crack extension in the PMMA layer varied from 12 mm for lower level of mixity ($s = 24$ mm) to 18 mm for higher mode mixity ($s = 4$ mm). The extent of crack growth in this case is less compared to the E–P plate. This is expected as the Epoxy crack is bridged from both sides by the un-cracked portion of the PMMA plates in this case. It can be observed from Fig. 11 that the crack front profile in the Epoxy layer is symmetric. Whereas, the crack in the PMMA layer advances more near the interface than in the interior of the plate. Once crack extension starts in one of the PMMA layers, the specimen failed suddenly. The failure of the layered plates therefore involves (i) crack initiation in the Epoxy layer at a load we designate as L_e, (ii) crack extension in the Epoxy layer with

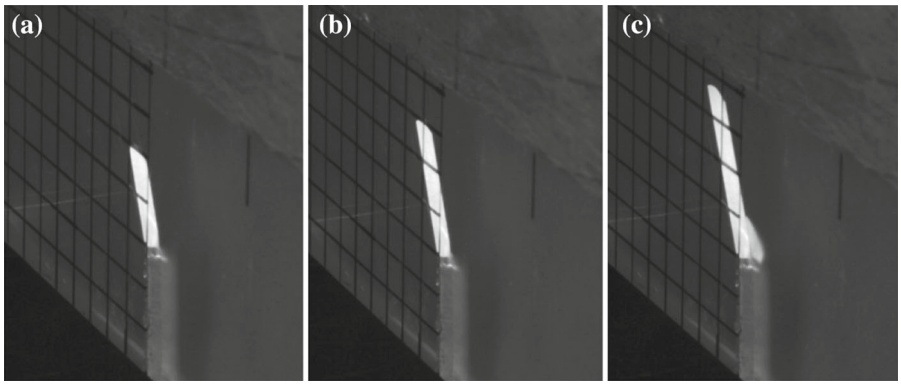

Fig. 10 Photographs showing stages of crack growth in E–P plate ($s = 24$ mm). **a** 1390 N, **b** 1460 N, **c** 1560 N

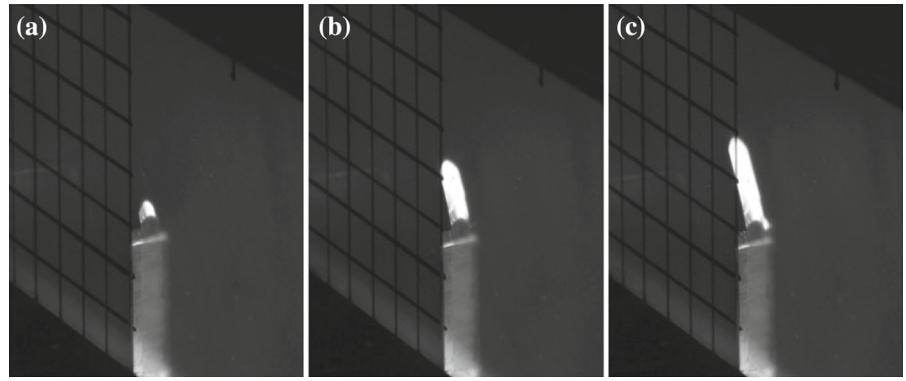

Fig. 11 Photographs showing stages of crack growth in P–E–P plate ($s = 20$ mm). **a** 1356 N, **b** 1899 N, **c** 2189 N

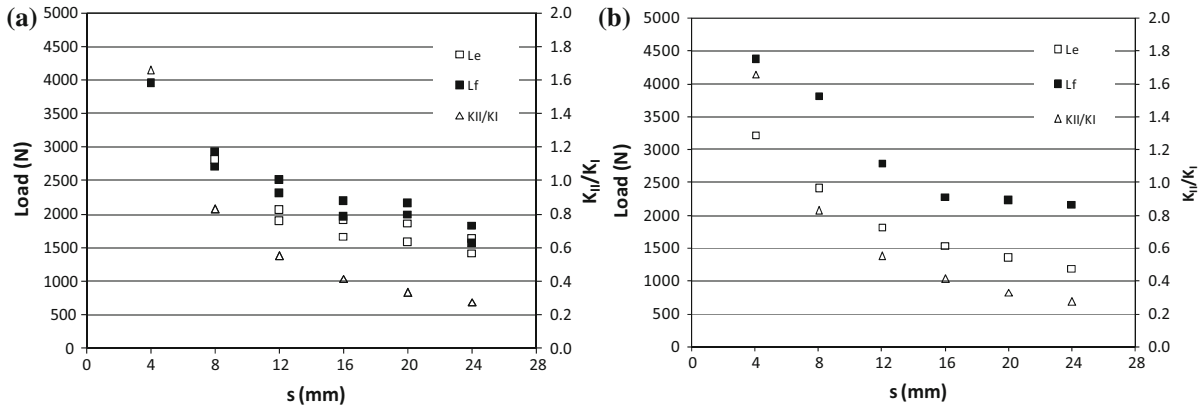

Fig. 12 Loads L_e and L_f as a function of the parameter s along with ratio of K_{II}/K_I for **a** E–P and **b** P–E–P plates

increase in load and (iii) final fracture of both layers on reaching the maximum load L_f.

Figure 12 shows the loads L_e and L_f along with K_{II}/K_I as a function of s for both E–P and P–E–P plates. In both cases, L_e and L_f increases with decreasing s i.e. with increasing mode mixity. In the case of E–P plate, the difference between L_f and L_e is not considerable whereas the same is not true for the P–E–P plate.

4.2 Fracture surface analysis

The fractured surface of the specimen was mapped using a three-axis coordinate measuring machine (Spectra 5.6.4. CNC). The measurement was performed over the entire surface by sampling the surface at 0.5 mm interval using a stylus of 1 mm tip radius. The entire data was then processed using Matlab to generate the profile of the fracture surface at different location along the crack path. The photograph of the fracture surface of E–P plate for $s = 8$ mm is shown in Fig. 13a. The coordinate reference used to define the profile is shown in the photograph. From Fig. 13a it can be observed that the angle of propagation is nearly same initially for both layers. For the two locations indicated by the two lines, marked 'a' and 'b' in Fig. 13a, the variation of Z along the plate thickness (X) is shown in Fig. 13b. Location 'a', is chosen such that it is within the stable crack extension zone for the Epoxy crack whereas location 'b' is in the region where both cracks extended simultaneously. Further it should be noted that for the sake of clarity, profiles are translated in such a way that the lowest point starts from $Z = 0.5$ mm in the case of location 'a' and from $Z = 1.5$ mm for the location 'b'. In Fig. 13b and d, the vertical dash-dot line indicates the interface. A profile nearly parallel to the X-axis indicates that the crack surface has not undergone any twisting. We can observe from Fig. 13b that at location 'a', the crack in the Epoxy layer has twist whereas that in the PMMA layer does not have any noticeable twist. At location 'b', crack in both layers has twist but of opposite nature. The photograph of the fractured

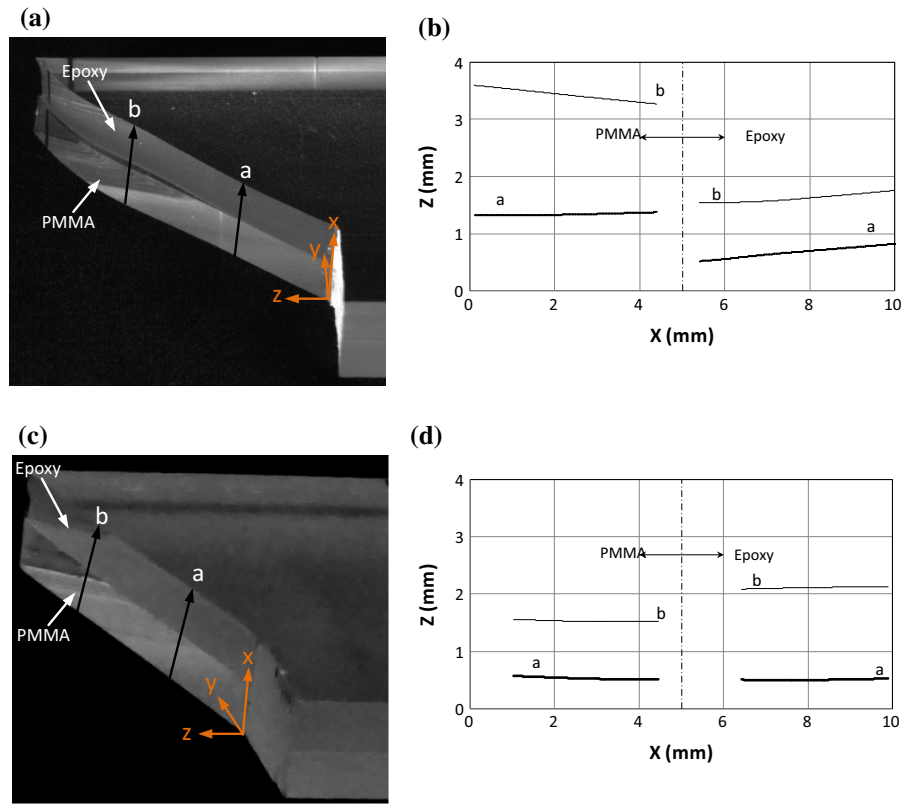

Fig. 13 Photograph of the fracture surface for **a** $s = 8$ mm and **c** $s = 24$ mm and corresponding surface profile **b** and **d** for E–P plate

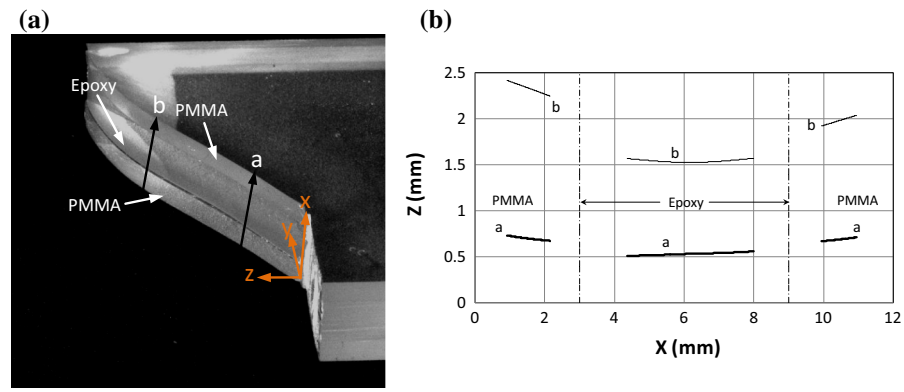

Fig. 14 Photograph of the fracture surface for **a** $s = 8$ mm and AFPB corresponding surface profile P–E–P plate

specimen and the corresponding surface profile for the E–P plate for $s = 24$ mm (low mode-II) are shown in Fig. 13c and d. At both locations 'a' and 'b', the crack has negligible twist. The surface profiles at locations 'a' and 'b' for the P–E–P plate for $s = 8$ mm, shown in Fig. 14b, indicate that there is crack twist in the PMMA layers at both locations, whereas the crack in the Epoxy layer has negligible twist. From the analysis of the fractured surfaces, it is obvious that the crack twist is higher in the case of $s = 8$ mm which corresponds to higher mode mixity. However, it should be noticed that in all cases, the overall level of crack twist is very small, in the range of 3-4 degrees. Therefore, one can assume that cracks in both layers follow nearly the same path.

5 Results of finite element analysis

In this section, the results of the FE analysis will be presented. Figures 15 and 16 show the variation of nor-

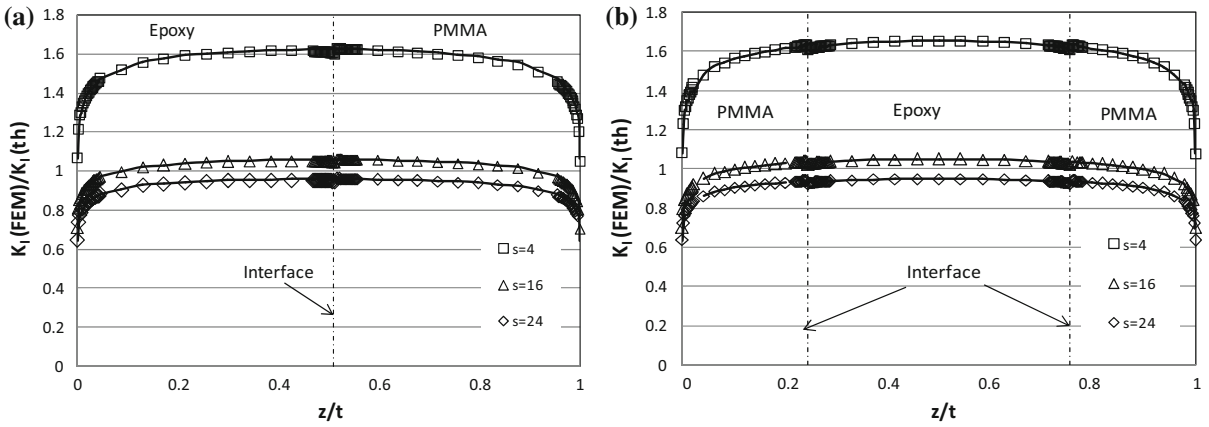

Fig. 15 Variation of K_I along the thickness of the layered plate

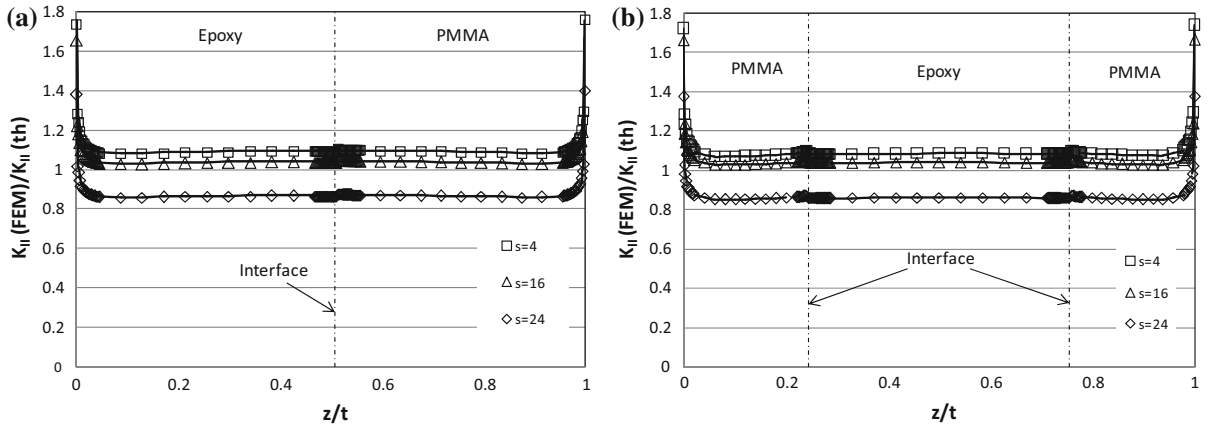

Fig. 16 Variation of K_{II} along the thickness of the layered plate

malized SIFs, K_I and K_{II}, along the crack front in E–P and P–E–P plates for three different loading conditions ($s = 4$, 16 and 24 mm). For normalizing the SIFs, K_I and K_{II} obtained from Eq. (1) are first scaled using Eq. (7) to obtain their respective values in each layer. Then the K_I and K_{II} obtained from FE analysis are normalized using the values calculated using Eqs. (1) and (7) for each layer. The variation of normalized K_I and K_{II} for a plate made of homogeneous material having modulus same as the equivalent modulus (Eq. 3) is also shown in Figs. 15 and 16 by the solid line for the three values of $s = 4$, 16 and 24 mm. The normalized K_I for the homogeneous plate varies across the thickness for all values of s considered. While there is considerable reduction of K_I near the free surfaces, K_I is nearly constant in the interior of the plate. On the contrary, K_{II} exhibits steep increase near the free surfaces and this behavior of K_I and K_{II} has been reported earlier (Nakamura and Parks 1988, 1989). For the E–P and P–E–P plate also, the variation of normalized K_I and K_{II} follows the same pattern as that for the homogeneous plate and in fact overlaps K_I and K_{II} of homogeneous plate for the three values of s.

From Fig. 15 it can be observed that for both layered and homogenous plate, the mid-thickness value of K_I is different from that calculated using Eq. (1). For $s = 24$ mm, Eq. (1) overestimates the mid-thickness value of K_I whereas Eq. (1) underestimates the mid-thickness value of K_I for $s = 4$ mm. Similar trend can be observed in Fig. 16 for K_{II} also. This explains the difference (see Fig. 9) between the thickness averaged SIFs obtained from the photoelastic fringes and that obtained from Eq. (1). It can be observed that the variation of the normalized SIFs for the layered plate

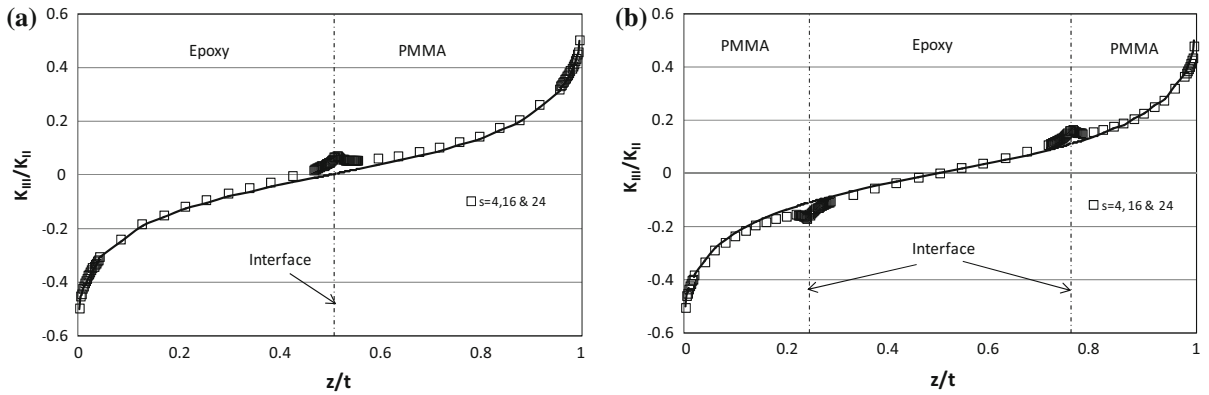

Fig. 17 Variation of K_{III}/K_{II} along the thickness of the layered plate

overlaps that for a homogeneous plate. This indicates that by using Eqs. (1) and (7), the individual layer SIFs for a layered plate can be calculated with the same level of accuracy as that obtained when using Eq. (1) for calculating the SIF in a homogeneous plate.

The FE analysis also revealed the existence of mode-III component of SIF, K_{III}. Figure 17 shows the variation of K_{III}/K_{II} across the thickness of layered plate along with that for an equivalent homogeneous plate (solid line). The fact that a K_{II} field induces a K_{III} field for a homogeneous plate has been reported earlier as well (Nakamura and Parks 1989). The curves for the layered plate for all values of s overlap that for the homogeneous plate indicating that the variation of K_{III}/K_{II} for the layered plate is same as that for the homogeneous plate. Further the curves for $s = 4$, 16 and 24 mm overlap each other indicating that the level of K_{III} is dependent only on the level of K_{II} which depends on the value of s. For smaller values of s, K_{II} will be higher and consequently K_{III} will be higher. This is the reason for the relatively higher crack twist observed in Sect. 4.2 in the case of $s = 8$ mm.

6 Discussion

The following salient observations can be made regarding the fracture behavior of the layered plates from the experimental results presented in Sect. 4; (i) the crack in the most brittle layer (Epoxy) starts extending upon reaching the load L_e, (ii) this crack extends to some length depending on the layer configuration and mode mixity, (iii) the PMMA layer crack starts extending at a load of L_f leading to final failure of the material (iv) L_f is significantly higher than L_e for the P–E–P plate and (v) the cracks in both layers follow nearly the same path. In this section, an attempt will be made to predict the failure of the plate using the MTS criteria. Since the twist angles observed are very small and the mode-III SIF is mostly due to parasitic effects, only opening and shear mode SIFs will be considered in the analysis. To accomplish this, the SIFs in each layer will be evaluated first using Eqs. (1) and (7). Thereafter using Eqs. (8–10), the direction of crack propagation and the load (L_e) at which the Epoxy crack will extend will be obtained. Comparison of the crack propagation angle calculated using the MTS criteria with that obtained from experiments is shown in Fig. 18a. Figure 18b shows the comparison of the load L_e calculated using the MTS criteria with that obtained from experiments. The two are in agreement indicating that by this approach, the crack propagation angle and the load at which the Epoxy crack will extend can be predicted for both E–P and P–E–P plates. The dotted line in Fig. 18b is the load at which a single layer of Epoxy plate, having thickness same as the total thickness of the layered plate, will fail. This load is higher than that for the layered plate as the elastic mismatch results in amplification of the SIFs in the stiffer Epoxy layer compared to a single Epoxy layer for the same applied load. However, in the case of a single Epoxy plate, once the crack starts extending it will grow unstably whereas in the layered plate this does not happen. Once the Epoxy crack has advanced, the SIFs at the tip of the PMMA crack cannot be evaluated using Eqs. (1) and (7).

The variation of load L_f for both E–P and P–E–P plate as a function of s is shown in Fig. 19.

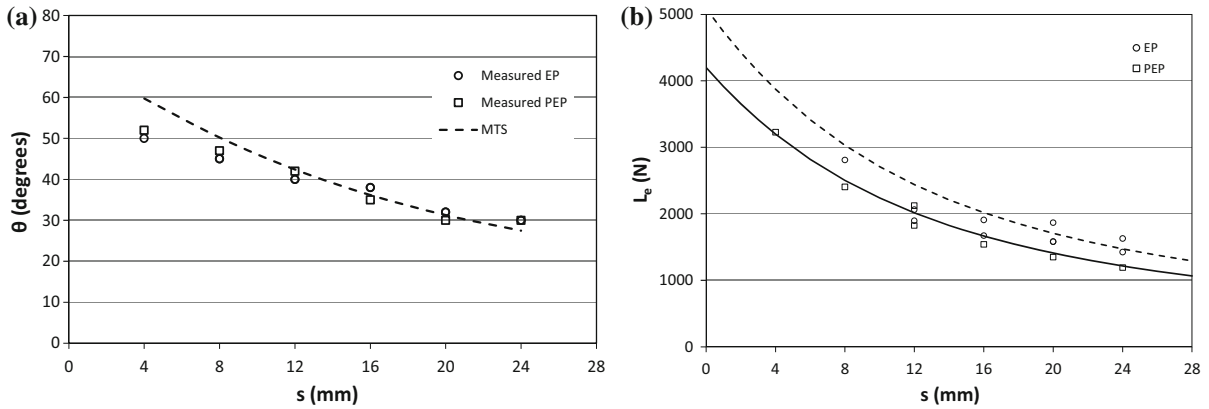

Fig. 18 **a** Crack initiation angle in Epoxy layer with for different values of s and **b** prediction of load at extension of Epoxy crack (L_e). The data is from both E–P and P–E–P plates. The *solid line* in **b** is the load at which the Epoxy crack starts extending in the layered plate. The *dotted line* in **b** is the load at which a single layer of Epoxy plate, having thickness same as the total thickness of the layered plate, will fail

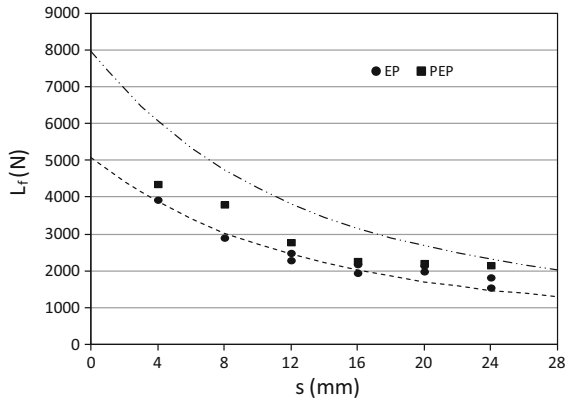

Fig. 19 Variation of L_f with s for E–P and P–E–P plates. The *dotted line* and the *dot-dash line* indicate the failure load respectively for Epoxy and PMMA plates each having thickness same as that of the total thickness of the layered plate

The dotted line and the dot-dash line are the failure load for Epoxy and PMMA plates each having thickness same as the total thickness of the layered plate. The final load L_f for the E–P plate is close to the failure load of a single Epoxy plate, indicating that this configuration has not improved the fracture tolerance. However, the same does not hold true for the P–E–P plate for which L_f is higher than L_e by 35% at higher mode mixity ($s = 4$ mm) and by 80% at lower mode mixity ($s = 24$ mm). The failure load L_f for the P–E–P plate is however lower than that of a single PMMA plate having thickness equal to the total thickness of the layered plate. Therefore, the strength of the cracked layered plate is lower than that of a cracked PMMA plate having identical thickness and crack length. However, it should be emphasized that due to layering, the overall stiffness of the plate is higher than the PMMA plate and the failure is not unstable as it would have been in a single Epoxy or PMMA plate. This is a one definite advantage over using a single layer.

Analytical prediction of the final load L_f is not easy due to the mechanics involved, which will be discussed in the rest of this section. Experimental results indicate that even after the crack in the Epoxy layer starts extending, the Epoxy layer continues to carry load because the un-cracked portion of the PMMA layer acts as a patch on the advancing Epoxy-layer crack tip. The effect of this is to reduce the SIF at the Epoxy crack-tip. As soon as critical condition is satisfied at the Epoxy crack-tip, the crack extends with a jump in the case of E–P plate. The closure forces exerted by the PMMA layer on the extended crack-tip will reduce the SIF leading to crack arrest. Since the test is a displacement-controlled test, with increase in displacement the load in the Epoxy layer increases resulting in the crack becoming critical again leading to further extension of the crack. This leads to the observed phenomenon of crack extension and arrest in the Epoxy layer until both layers fail. In the case of P–E–P plate, since the PMMA layer patches the Epoxy crack from both sides, the crack grows more stably and to a lesser length before final failure.

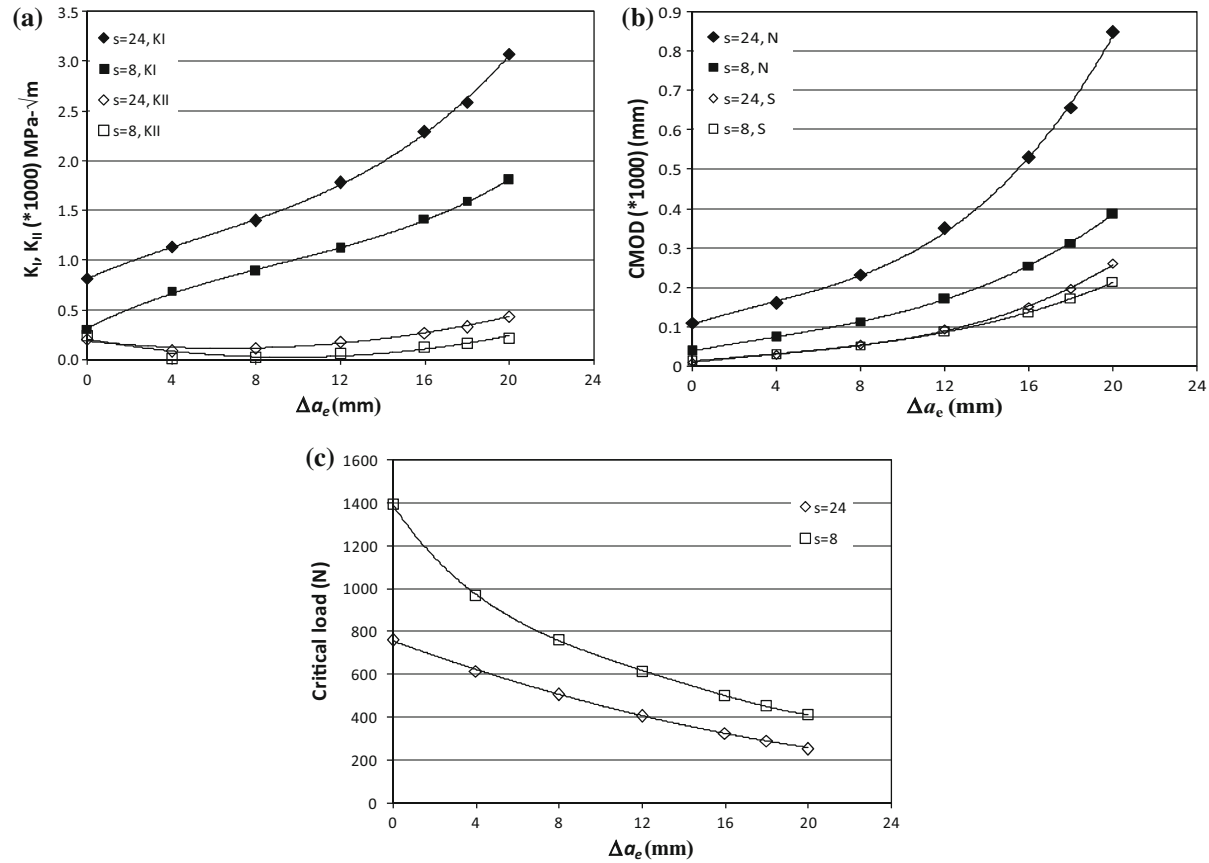

Fig. 20 Variation of **a** SIF, **b** crack mouth opening (N- normal & S-sliding) and **c** critical load as a function of crack extension in the Epoxy layer

To understand the interaction between the layers, the two layers will be analyzed individually. The critical load for a single Epoxy layer of thickness 5.8 mm having a crack kinked at an angle same as that observed in experiments was evaluated for the two cases of $s = 8$ and 24 mm. To calculate this load, first, a 2D finite element analysis was performed to evaluate the SIFs for a unit load and thereafter using this information and MTS criteria, the load was calculated for different crack extension. Figure 20a and b show the SIFs and crack mouth opening displacements (CMOD) respectively for a unit load and Fig. 20c shows the critical load all of them as a function of crack extension Δa_e, for the two cases of $s = 8$ and 24 mm. It can be easily observed from Fig. 20a that the crack is predominantly under opening mode. This is also indicated by the photoelastic fringes shown in Fig. 8b. Further, for the same load and crack length, the opening mode SIF is higher in the case of $s = 24$ mm when compared to $s = 8$ mm. Similar is the case with CMOD shown in Fig. 20b. As one would expect, the critical load decreases with crack extension as shown in Fig. 20c. However it should be noticed that for the same crack length, the critical load for continued crack extension in the Epoxy layer is higher in the case of $s = 8$ mm when compared to $s = 24$ mm.

Before the extension of the Epoxy crack happens the CMOD can be assumed to be same for both layers (corresponding to $\Delta a_e = 0$). Once the Epoxy crack extends, the CMOD for this layer will increase and this will be restricted by the PMMA layer. This will lead to reduction of SIF at the Epoxy crack tip, however, at the cost of an increase of SIF at the PMMA layer crack tip compared to the situation in which the two layers behaving independent of each other. It should be observed that for the same crack length and load,

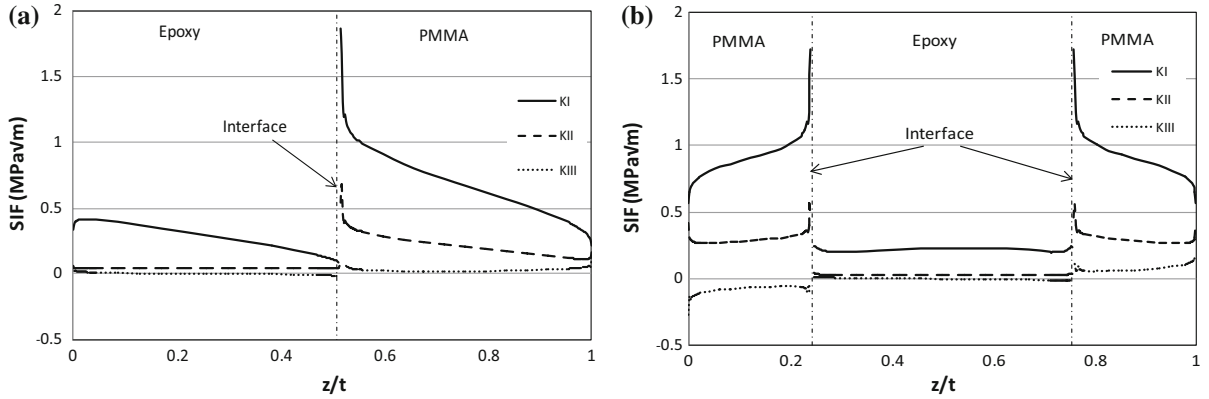

Fig. 21 Variation of SIF just before crack extension in the PMMA layer for $s = 24$ mm. **a** E–P, **b** P–E–P

the CMOD is higher in the case of $s = 24$ mm when compared to $s = 8$ mm. Because of this, during the layer interactions, the increase in SIF at the PMMA crack will be higher for the case of $s = 24$ mm when compared to $s = 8$ mm. This implies that the reduction of the load carrying capacity of the PMMA layer due to the layer interactions is higher in the case of $s = 24$ mm when compared to $s = 8$ mm.

The variation of the SIFs in the layers obtained from the FE simulations (Fig. 6) is shown for E–P and P–E–P plates in Fig. 21 for $s = 24$ mm. The Epoxy crack length and load used in this analysis correspond to that just before the extension of the PMMA crack. In E–P plate, K_I decreases steeply from the free surface to interface due to the closing traction applied by the PMMA layer. On the contrary, K_I increases towards the interface in the PMMA layer. In P–E–P plate, the closing traction on the Epoxy crack is exerted on both sides resulting in lesser variation of K_I about the mid plane in the Epoxy layer. The interesting fact to be observed from Fig. 21 is that the SIF in the Epoxy layer is less than the K_{IC} of Epoxy, where as that in the PMMA layer is higher than the K_{IC} of PMMA especially near the interface. Extension of the PMMA crack started near the interface in the experiments (Fig. 10). This suggests that at this load, the PMMA crack starts extending first followed by the Epoxy crack.

In both E–P and P–E–P plates K_{II} in the Epoxy layer is very low and remains nearly constant through the crack front. Figure 22 shows the variation of ratio of K_{II}/K_I along the crack front. There is significant variation of K_{II}/K_I along the crack front in the Epoxy layer whereas K_{II}/K_I is constant in the PMMA layer and the value is close to that given in Fig. 12. This explains the experimental observation of both Epoxy and PMMA cracks extending along the same direction initially. The load shared by the Epoxy plate and the PMMA plate for $s = 24$ mm just before the PMMA crack becomes critical was determined from FE analysis. The loads on the Epoxy and PMMA layers were respectively 868 and 632 N for the E–P plate and for P–E–P plate, the loads were 1237 and 863 N. Comparison of the Epoxy layer load with that shown in Fig. 20c would indicate that these loads are considerably higher than the critical load for a single Epoxy layer. On the contrary, the critical load for a single PMMA layer of 5.5 mm thickness calculated using MTS criteria is 1026 N for $s = 24$ mm which is higher than the load shared by the PMMA plate in the layered configuration at the point of final failure. This implies that the PMMA crack becomes unstable at a load well below the critical load for this layer. The reason for this was explained earlier. Because of this reason L_f is less than the failure load for a single PMMA plate of thickness same as the total thickness of the layered plate.

Based on the findings of this study, which are for a particular system (Epoxy/PMMA), some insights on the behavior of a more general case can be deduced as follows. The amplification of SIF in the stiffer layer depends entirely on the ratio (α) of elastic modulus of the stiffer layer (E_s) to the equivalent elastic modulus (E_{eq}). The equivalent elastic modulus depends on the ratio of the layer elastic moduli (β) and the ratio of layer thicknesses. Assuming in general that a stiffer material is also more brittle, Eq. (7) would indicate that the load at which a crack initiates in the stiffer layer (L_s) would

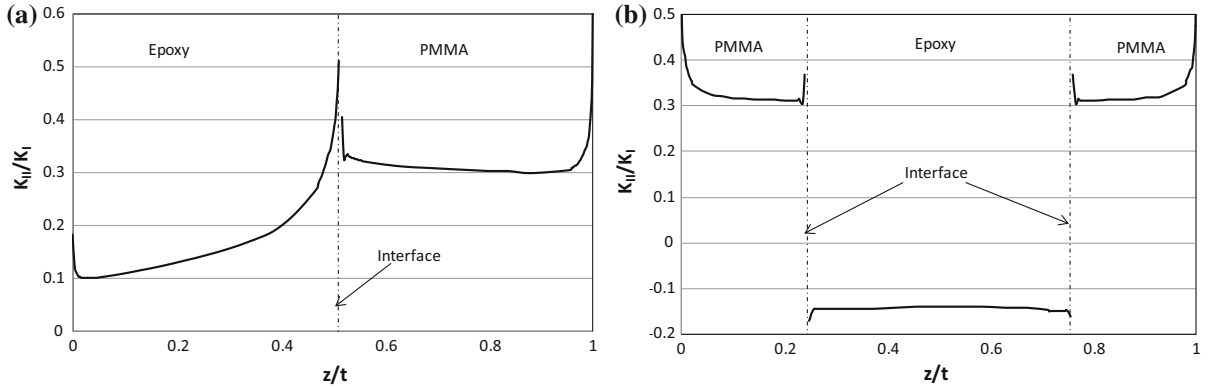

Fig. 22 Variation of K_{II}/K_I just before crack extension in the PMMA layer for $s = 24$ mm**a** E–P, **b** P–E–P

be always less than the load (L) at which a crack in an identical plate made entirely of the stiffer material would initiate. The ratio of these two loads (L_s/ L) scales inversely with α. For a given β and total plate thickness, reducing the thickness of stiffer layer will result in increasing α and decreasing the fracture load L_s. The final failure load (L_f) depends on the fracture toughness and thickness of the less stiff layer. This load will be less than the failure load of a plate made entirely of the less stiff material having thickness same as that of the layered plate (please see Fig. 19). We would surmise that reducing the thickness of the less stiff layer would reduce L_f. Therefore, a balanced option would be to have same thickness for the two layers in which case, the equivalent stiffness will be higher than that of the less stiff material and the final failure load (L_f) would be higher than that of the more brittle layer.

7 Conclusions

The fracture behavior of edge cracked layered plates having property jumps across the crack front was investigated under mixed mode loading. Two layer and three layer plates comprising of layers made of Epoxy and PMMA were considered. The plates having initial cracks of the same length were subjected to mixed mode loading. The experimental part of the study indicated that the layered plates exhibited a progressive type of failure in which the crack in the relatively stiffer and brittle Epoxy layer first started extending and grew stably to some length before the final catastrophic failure of the plate. It was observed that there are two critical loads, one (L_e) at which the Epoxy layer crack starts extending and the other (L_f) at which final failure occurs. The cracks in both layers had the same initial kink angle and followed nearly similar paths, even though they extended at different instants. The crack surfaces had small amount of twist. For the two-layer configuration (E–P), the difference between L_f and L_e was small and therefore L_e can be conservatively considered as the fracture strength of the plate. L_e is found to increase with increasing mode mixity. On the contrary, for the three layer (P–E–P) plate L_f was higher than L_e, however the percentage increase over L_e decreased with increasing mode mixity. This implies that for the P–E–P plate, the relative strength enhancement due to layering is higher at lower mode mixity.

From the results of the FE analysis it was observed that the SIFs vary across the crack front. For the same load, SIF in the stiffer layer of the layered plate was higher compared to that for a monolitihc plate having the same total thickness as the layered plate. The existing equations relating SIF to far field load for a monolithic plate, obtained based on two-dimensional analysis, can also predict the SIF in the layered plate with reasonable accuracy. However, these equations ignore the mode-III component of the SIF present in both monolithic and layered plates, which explains the small level of twist observed in the crack surfaces. It was observed that layering did not have any effect on the extent of mode-III component.

The load (L_e) at which Epoxy crack initiates predicted using the MTS criteria matched reasonably well with the experimental values. The results of the FE analysis also indicated that while the PMMA layer decreases the SIF at the Epoxy crack front once this

crack started extending, the larger CMOD of the Epoxy layer resulted in increase in the SIF at the PMMA crack tip. This resulted in reducing the load carrying capacity of the PMMA layer in the layered configuration when compared to a monolithic layer of PMMA. However, prediction of L_f needs crack growth analysis in the Epoxy layer, which is beyond the scope of this study. In summary, by layering the stiffness of the plate can be improved in comparison to that of the relatively compliant plate both in the two-layer and three-layer configuration. While in both cases, the failure is progressive in nature compared to a monolithic construction the strength in both configurations is less than that of a monolithic plate made of PMMA, the relatively tougher material among the two. Based on the observations for this particular material system, insights on the behavior of a general system are also provided.

Acknowledgments The authors acknowledge the financial support of Aeronautical Research and Development Board, India through grant number DARO/08/1051679/M/I.

References

Badaliance R, Sih GC (1975) An approximate three-dimensional theory of layered plates containing through thickness cracks. Eng Fract Mech 7:1–22. doi:10.1016/0013-7944(75)90063-6

Bankar UH, Parameswaran V (2013) Fracture of edge cracked layered plates subjected to in-plane bending. Exp Mech 53:287–298. doi:10.1007/s11340-012-9649-6

Dally JW, Riley WF (1978) Experimental stress analysis. McGraw-Hill, New York

Erdogan F, Biricikoglu V (1973) Two bonded half planes with a crack going through the interface. Int J Eng Sci 11:745–766. doi:10.1016/0020-7225(73)90004-9

Hutchinson JW, Suo Z (1992) Mixed mode cracking in layered materials. Adv Appl Mech 29:63–190

Kidane A, Shukla A (2010) Quasi-static and dynamic fracture initiation toughness of Ti/TiB layered functionally graded material under thermo-mechanical loading. Eng Fract Mech 77:479–491. doi:10.1016/j.engfracmech.2009.10.006

Kommana R, Parameswaran V (2009) Experimental and numerical investigation of a cracked transversely graded plate subjected to in plane bending. Int J Solids Struct 46:2420–2428. doi:10.1016/j.ijsolstr.2009.01.026

Kumar P (2009) Elements of fracture mechanics. Tata McGraw-Hill Education, New Delhi

Liu C, Lambros J, Rosakis AJ (1993) Highly transient elastodynamic crack growth in a bimaterial interface: higher order asymptotic analysis and optical experiments. J Mech Phys Solids 41:1887–1954. doi:10.1016/0022-5096(93)90074-P

Maccagno TM, Knott JF (1989) The fracture behaviour of PMMA in mixed modes I and II. Eng Fract Mech 34:65–86. doi:10.1016/0013-7944(89)90243-9

Moran B, Shih CF (1987) Crack tip and associated domain integrals from momentum and energy balance. Eng Fract Mech 27:615–642. doi:10.1016/0013-7944(87)90155-X

Nakamura T, Parks D (1988) Three-dimensional stress field near the crack front in a thin elastic plate. J Appl Mech 55:805–813

Nakamura T, Parks DM (1989) Antisymmetrical 3-D Stress field near the crack front of a thin elastic plate. Int J Solids Struct 25:1411–1426

Parameswaran V, Shukla A (1998) Dynamic fracture of a functionally gradient material having discrete property variation. J Mater Sci 33:3303–3311. doi:10.1023/A:1013277011848

Rice JR, Sih GC (1965) Plane problems of cracks in dissimilar media. J Appl Mech 32:418–423

Shukla A, Kavaturu M (1998) Opening-mode dominated crack growth along inclined interfaces: experimental observations. Int J Solids Struct 35:3961–3975. doi:10.1016/S0020-7683(97)00193-5

Shukla A (2001) High-speed fracture studies on bimaterial interfaces using photoelasticity—a review. J Strain Anal Eng Des 36:119–142. doi:10.1243/0309324011512658

Singh RP, Kavaturu M, Shukla A (1997) Initiation, propagation and arrest of an interface crack subjected to controlled stress wave loading. Int J Fract 83:291–304. doi:10.1023/A:1007358901588

Singh RP, Shukla A (1996) Subsonic and intersonic crack growth along a bimaterial interface. J Appl Mech Trans Asme. doi:10.1115/1.2787247

Singh RP, Parameswaran V (2003) An experimental investigation of dynamic crack propagation in a brittle material reinforced with a ductile layer. Opt Lasers Eng 40:289–306. doi:10.1016/S0143-8166(02)00089-1

Tippur HV, Rosakis AJ (1991) Quasi-static and dynamic crack growth along bimaterial interfaces: a note on crack-tip field measurements using coherent gradient sensing. Exp Mech 31:243–251. doi:10.1007/BF02326067

Walters MC, Paulino GH, Dodds RH Jr (2004) Stress-intensity factors for surface cracks in functionally graded materials under mode-I thermomechanical loading. Int J Solids Struct 41:1081–1118. doi:10.1016/j.ijsolstr.2003.09.050

Walters MC, Paulino GH, Dodds RH (2005) Interaction integral procedures for 3-D curved cracks including surface tractions. Eng Fract Mech 72:1635–1663. doi:10.1016/j.engfracmech.2005.01.002

Xu L, Tippur HV (1995) Fracture parameters for interfacial cracks: an experimental-finite element study of crack tip fields and crack initiation toughness. Int J Fract 71:345–363

Yang W, Suo Z, Shih CF (1991) Mechanics of dynamic debonding. Proc R Soc Lond Ser Math Phys Sci 433:679–697. doi:10.1098/rspa.1991.0070